Letter

Herding of proteins by the ends of shrinking polymers

Amer Al-Hiyasat [1,2] Yazgan Tuna [1], Yin-Wei Kuo [1], and Jonathon Howard[1,*]

[1]*Department of Molecular Biophysics and Biochemistry, Yale University, New Haven, Connecticut 06511, USA*
[2]*Department of Physics, Massachusetts Institute of Technology, Cambridge, Massachusetts 02139, USA*

The control of biopolymer length is mediated by proteins that localize to polymer ends and regulate polymerization dynamics. Several mechanisms have been proposed to achieve end localization. Here, we propose a novel mechanism by which a protein that binds to a shrinking polymer and slows its shrinkage will be spontaneously enriched at the shrinking end through a "herding" effect. We formalize this process using both lattice-gas and continuum descriptions, and we present experimental evidence that the microtubule regulator spastin employs this mechanism. Our findings extend to more general problems involving diffusion within shrinking domains.

Regulating the length of biological polymers is essential for myriad cellular processes such as mitosis, muscle contraction, and ciliary motility [1]. This regulation is often mediated by proteins that localize to polymer ends, where they promote or inhibit polymerization or depolymerization [2]. The mechanisms of protein end-localization on growing polymers such as microtubules and actin filaments have been well documented both experimentally and theoretically. Some proteins bind directly to ends from solution [3,4], some bind the polymer near the end and undergo one-dimensional diffusion to reach the end [5–7], and others are carried to ends by motor proteins [8–10]. Much less is known, however, about the localization of proteins to shrinking ends.

Microtubule severing proteins such as spastin and katanin cut microtubules along their lengths using the energy of ATP hydrolysis [11]. In addition to severing, both spastin and katanin promote "rescue," the conversion of shrinking microtubule ends to growing ones. This activity amplifies the microtubule mass [12,13], which is critical to spastin's biological function in cells (reviewed in Ref. [14]). Spastin is significantly enriched on shrinking microtubule ends, where it slows the shrinkage rate and facilitates the regrowth-promoting activity [15]. The mechanism of spastin's end-enrichment is unknown. Although many microtubule-associated proteins (MAPs) diffuse on microtubules (MTs), most fall off with depolymerizing subunits and do not enrich at shrinking ends. Examples include tau [16,17] and kinesins 8 and 13 [18].

End localization by spastin is not likely to involve direct binding or diffusion-and-capture: these would require very high attachment rates and diffusion coefficients to target shrinking ends, which move 10- to 40-fold faster than growing ones [15]. A potential mechanism is that spastin uses multivalent interactions (avidity) with the microtubule to maintain contact with the depolymerizing end [19]. This is thought to occur for end-tracking multiprotein complexes such as NDC80 [20,21], the DASH/Dam1 complex [22], and Kar9 [23]. Engineered [24] and synthetic oligomers [25] can

also possessively track shrinking ends, and depolymerizing kinesins have been proposed to do so as well [9]. While processive tracking cannot be ruled out for spastin, whose hexameric form cuts microtubules, there is no evidence that spastin end-localization requires oligomerization, and indeed spastin diffuses along microtubules as a monomer and localizes to their ends at low concentration [15].

In this Letter, we present a novel theoretical mechanism of shrinking-end localization that requires neither multivalent interactions, diffusive capturing, nor directed motility. We show that a protein that binds to a shrinking polymer and slows its shrinkage will be spontaneously enriched at the shrinking end due to a purely kinetic "herding" effect. This behavior is counterintuitive because one might expect that slowdown is driven by end enrichment, not the other way around. We experimentally demonstrate that spastin's end enrichment is quantitatively explained by this herding theory. In addition to providing insight into spastin's regulatory function, our results extend to a more general class of problems in which diffusive particles hinder the boundaries of a shrinking domain.

Mathematical model. We use a lattice-gas model to describe the shrinking polymer as a semi-infinite one-dimensional lattice situated in a reservoir of soluble protein (Fig. 1) [5,9,26,27]. Proteins from solution bind vacant lattice sites at a rate $\omega_a c$, where c is the concentration of protein in solution. Lattice-bound proteins can detach at a rate ω_d or hop to adjacent vacant sites at a rate ω_h in either direction. Shrinkage of the polymer occurs via the loss of lattice sites from the end at a rate ω_0 or ω_1, depending on whether the site at the end is vacant or occupied, respectively. We are interested in the case $\omega_1 < \omega_0$, corresponding to a slowing of shrinkage by the protein.

The state of the system is described by the set of occupancy numbers $\{n_i\}$ where $n_i = 1$ if the ith site is occupied and $i = 1$ corresponds to the shrinking end. Under these definitions, the time evolution of the mean occupancy at the end $\langle n_1 \rangle(t)$ obeys

$$\frac{d\langle n_1 \rangle}{dt} = \omega_h(\langle n_2 \rangle - \langle n_1 \rangle) + \omega_a c \langle 1 - n_1 \rangle - \omega_d \langle n_1 \rangle$$
$$+ \omega_0 \langle (1 - n_1)(n_2 - n_1) \rangle + \omega_1 \langle n_1(n_2 - n_1) \rangle. \quad (1)$$
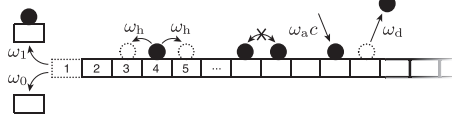
FIG. 1. Microscopic model of protein dynamics on shrinking polymer. The site at $i = 1$ dissociates with rate ω_0 if it is vacant and ω_1 if it is occupied.

Similarly, the mean occupancy of all other sites $i > 1$ follows

$$\frac{d\langle n_i \rangle}{dt} = \omega_{\mathrm{h}}(\langle n_{i+1} \rangle - 2\langle n_i \rangle + \langle n_{i-1} \rangle) + \omega_{\mathrm{a}}c\langle 1 - n_i \rangle$$
$$- \omega_{\mathrm{d}}\langle n_i \rangle + \omega_0\langle(1 - n_1)(n_{i+1} - n_i)\rangle$$
$$+ \omega_1\langle n_1(n_{i+1} - n_i)\rangle. \quad (2)$$

Equations (1) and (2) are derived in Sec. I of the Supplemental Material (SM) [28]. Due to the moving frame, there is an apparent advection of particles towards the shrinking end at $i = 1$.

In the case $\omega_0 = \omega_1$ (no slowdown by end-occupancy), equations (1) and (2) have the stationary solution

$$\langle n_i \rangle = \frac{\omega_{\mathrm{a}}c}{\omega_{\mathrm{a}}c + \omega_{\mathrm{d}}} = \rho_\infty$$

for all i. This is the *Langmuir isotherm*, the density for a polymer that is in equilibrium with the protein bath and fixed in length. For $\omega_0 \neq \omega_1$, direct solution of equations (1) and (2) is complicated by the presence of correlations between n_1 and the other sites, but we can invoke a mean-field (MF) approximation $\langle n_1 n_i \rangle \approx \langle n_1 \rangle \langle n_i \rangle$. The continuum limit of the lattice model is then

$$\partial_{\bar{t}}\rho(\bar{x}, \bar{t}) = \overline{D}\,\partial_{\bar{x}}^2\rho(\bar{x}, \bar{t}) + [1 - (1 - \bar{v}_1)\rho(0, \bar{t})]\partial_{\bar{x}}\rho(\bar{x}, \bar{t})$$
$$+ \bar{k}\bar{c}[1 - \rho(\bar{x}, \bar{t})] - \bar{k}\rho(\bar{x}, \bar{t}), \quad (3)$$

where we have defined the continuous spatial variable $\bar{x} = i - 1$ as well as the dimensionless time $\bar{t} = t\omega_0$, which normalizes the natural polymer shrinkage rate to unity. The mean linear density of protein on the polymer is $\rho(\bar{x}, \bar{t}) = \langle n_{(x+1)} \rangle(\bar{t}/\omega_0)$. We further define $\overline{D} = \omega_{\mathrm{h}}/\omega_0$, the ratio of the hopping rate to the natural shrinkage rate, $\bar{k} = \omega_{\mathrm{d}}/\omega_0$, the dimensionless detachment rate of the protein, and $\bar{c} = \omega_{\mathrm{a}}c/\omega_{\mathrm{d}}$, which determines the Langmuir isotherm $\rho_\infty = \bar{c}/(1 + \bar{c})$. Lastly, we define a slowdown parameter $\bar{v}_1 = \omega_1/\omega_0$ controlling the extent to which the protein slows shrinkage. When $\bar{v}_1 = 0$, depolymerization is only possible when the terminal site is vacant, and when $\bar{v}_1 = 1$, the depolymerization rate is unaffected by end occupancy. From equation (3), we identify the measured shrinkage velocity of the microtubule

$$\bar{v}(\bar{t}) = 1 - (1 - \bar{v}_1)\rho(0, \bar{t}).$$

Far from the shrinking end, the density of the protein is the equilibrium Langmuir density ρ_∞. With this boundary condition, stationary solutions to equation (3) take the form of an exponential decay with the distance from the end,

$$\rho(\bar{x}) = [\rho(0) - \rho_\infty]e^{-\lambda\bar{x}} + \rho_\infty, \quad (4)$$

where

$$\lambda = \frac{1 - (1 - \bar{v}_1)\rho(0) + \sqrt{4\overline{D}\,\bar{k}(1 + \bar{c}) + [1 - (1 - \bar{v}_1)\rho(0)]^2}}{2\overline{D}}.$$

To set the boundary condition at the shrinking end, we note that the microscopic model has no binding sites to the left of $\bar{x} = 0$, and so the end must be reflecting. This gives

$$-\overline{D}\,\partial_{\bar{x}}\rho(0) - \bar{v}\rho(0, \bar{t}) = \bar{k}\bar{c}[1 - \rho(0)] - (\bar{k} + \bar{v}_1)\rho(0), \quad (5)$$

where we have imposed that the total flux (diffusive and advective) through the end must equal the net binding or detachment at the end. This condition can be used together with equation (4) to express $\rho(0)$ as the root of a cubic polynomial (SM, Sec. II [28]). Notably, the solutions predict $\rho(0) > \rho_\infty$, implying that there is an enrichment of the protein at the shrinking filament end. Simulations of the microscopic model using the Gillespie algorithm predict that the mean lattice occupancies approach a steady state that is in good agreement with the stationary solution of the mean-field model [Fig. 2(a)]. This agreement is robust against changes in the parameters (Fig. S1 [28]).

The gradual accumulation at the end is due to a "herding" effect, where the shrinking end slows when it encounters a protein and then speeds up again when the protein hops away from the end along the lattice. The result is a buildup of the protein near the reflecting end. This unexpected behavior, where slowdown causes end enrichment and not vice versa, depends strongly on the extent of slowdown: the enrichment is maximum when $\bar{v}_1 = \omega_1 = 0$ [Fig. 2(b)]; that is, when a protein in the $i = 1$ site completely pauses depolymerization. Since every lattice site is indistinguishable to the protein, herding is a purely kinetic effect. If $\overline{D}$ or $\bar{k}$ are too large, the proteins achieve diffusive or Langmuir equilibrium between lattice-depolymerization events, preventing end enrichment [Fig. 2(c)]. This is in contrast with diffusion-and-capture mechanisms, in which a large diffusion coefficient increases the end localization rather than decreasing it [5], or to direct-binding mechanisms, in which fast lattice turnover promotes end enrichment. A consequence of herding is that far less protein is needed on the lattice in order to impart a certain level of shrinkage slowdown [Fig. 2(d)].

Application to spastin. To test whether spastin employs the herding mechanism to enrich at shrinking ends, we used the *in vitro* reconstitution assay described in Ref. [29] to study green fluorescent protein–labeled [(GFP)-labeled] spastin. Experimental details are provided in Sec. IV of the SM. Briefly, we grew GMPCPP-stabilized microtubule "seeds," which do not shrink, and immobilized them on a functionalized surface within a microfluidic flow chamber. We perfused in a tubulin and GTP-containing solution, which causes dynamic microtubule extensions to grow from the ends of the seeds. We then perfused tubulin, GTP, and GFP-spastin, allowing spastin to decorate the dynamic microtubules and reach its equilibrium density. To prevent severing, no ATP was included. Finally, we perfused a solution containing spastin but no tubulin. The removal of tubulin induces "catastrophe" events, whereby growing ends switch to shrinking ones. GFP-spastin was visualized using total-internal-reflection fluorescence (TIRF)-microscopy [30]. In all microtubules observed ($n > 200$),
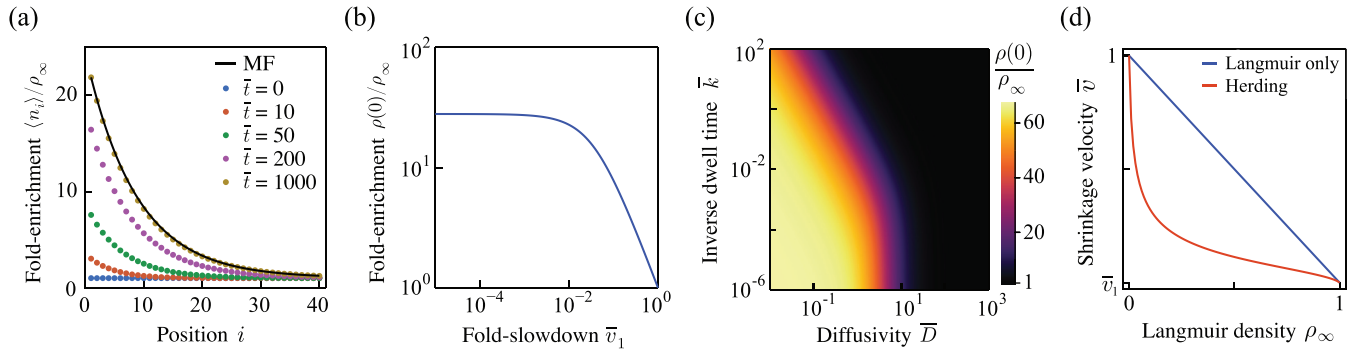
FIG. 2. Herding theory of protein enrichment at shrinking ends. (a) Occupancy probability at each position at different times. Circles: simulations of the lattice-gas model. Line: mean-field solution. Fold enrichment at the end as a function (b) of $\bar{v}_1 = \omega_1/\omega_0$ and (c) of $\overline{D}$ and $\bar{k}$. (d) Mean shrinkage velocity as a function of the equilibrium protein density.

robust end enrichment was evident [Fig. 3(a)]. Enrichment occurs on both ends of a shrinking microtubules (Fig. S2 [28]). This experiment confirms that spastin concentrates on depolymerizing ends. We then asked whether the enrichment is due to spastin preferentially binding to the end from solution or if it is due to the sweeping of lattice-bound spastin. To this end, we employed a "wash-out" assay, where spastin was loaded onto microtubules in the presence of tubulin, and then both tubulin and spastin were washed out. This induces catastrophe within a spastin-free solution. We found that spastin was still enriched at shrinking ends [Fig. 3(b)]. This conclu-
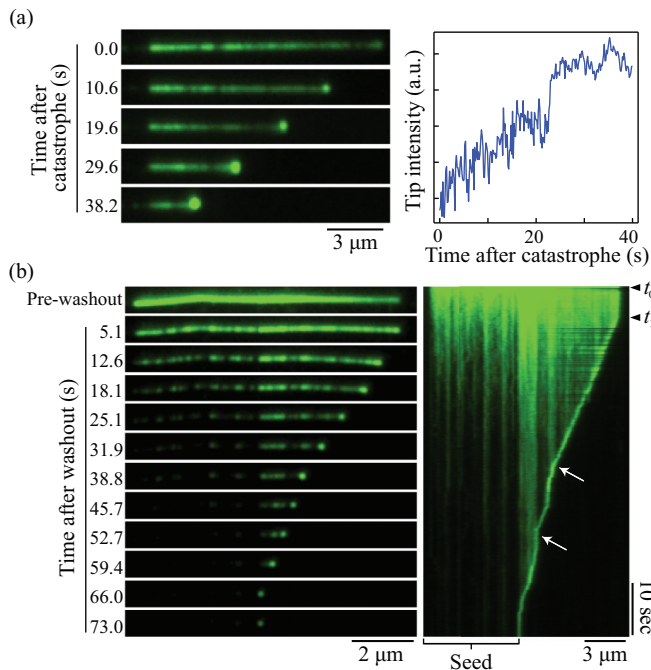

FIG. 3. Dynamics of GFP-spastin on shrinking microtubules observed via TIRF microscopy. (a) Accumulation of spastin on shrinking ends: (left) representative time series, (right) end intensity trace generated by integrating a $1\,\mu\text{m}^2$ region centered at the end. (b) Washout assay showing end enrichment without spastin in solution: (left) representative time series, (right) kymograph. t_0 is the washout time and t_1 is the catastrophe time. Arrows indicate slowdown of shrinkage.

sively demonstrates that a direct-binding EB1-like mechanism [3] is not necessary for end enrichment. Indicated on the kymograph (white arrows) are points where the end slows down when encountering regions of high spastin density and then speeds up again when spastin detaches. This indicates a negative correlation between end occupancy and shrinkage speed, supporting the herding effect. These results show that the shrinking end sweeps up spastin as it moves.

To quantitatively test our theory, we directly measured spastin's attachment rate k_a, detachment rate k_d, and diffusion coefficient D. The conversion to the model parameters ($\overline{D}$, $\bar{c}$, and $\bar{k}$) is given in Table S2 [28]. The attachment rate was estimated by counting single-molecule landing events at 10 nM GFP-spastin. This yielded $k_a = (0.031 \pm 0.002)\ \mu\text{m}^{-1}\,\text{nM}^{-1}\,\text{min}^{-1}$ (mean $\pm$ standard error; 153 events). To measure the diffusion coefficient and detachment rate, we performed a washout assay using a low initial concentration to visualize single-molecule trajectories (Fig. S3 [28]). The spastin dwell time was exponentially distributed [Fig. S4(a) [28]] with an estimated mean $1/k_d = (17.7 \pm 1.4\ \text{s})$ (158 events). Diffusion coefficients were estimated on a per-trajectory basis and fell into a broad range [Fig. S4(b) [28]], with a median of $D = 0.008\,\mu\text{m}^2\,\text{s}^{-1}$ (interquartile range: 0.008). These parameter values are similar to those measured for human spastin [31].

We next measured the microtubule shrinkage velocity v as a function of the concentration of spastin in solution c (Fig. 4, circles). The $v(c)$ curve allows an estimation of the slowdown parameter $\bar{v}_1$ as the ratio $v(\infty)/v(0)$, where $v(\infty)$ is the saturating shrinkage velocity at high concentrations. Using the measurement at 1000 nM, we can place an upper bound at $\bar{v}_1 = 0.04$. Curve fitting suggests that the true value is even closer to zero. Thus, we were able to measure the key parameters in the model.

To make model predictions, we calculated the dimensionless parameters using a lattice spacing of 8 nm and the measured value $v_0 = 28.0\,\mu\text{m}\,\text{min}^{-1}$, corresponding to $\omega_0 = 58.3\,\text{s}^{-1}$. The results are $\bar{k} = 0.0010 \pm 0.0002$, $\overline{D} \leqslant 2.0 \pm 0.5$, and $\bar{v}_1 \leqslant 0.04$. This places spastin in a region where herding is expected to be significant [Figs. 2(b) and 2(c)]. At 50 nM, the enrichment at the end is at least 21-fold and likely closer to 200-fold. The width of the enriched region is on the order 8 nm/λ = 75 nm, which is below the diffraction limit and in agreement with experiments.
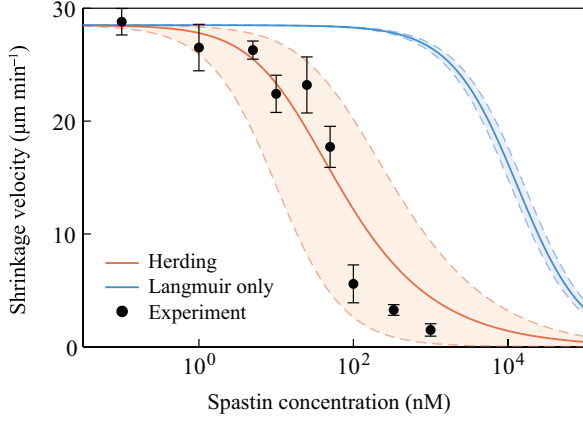
FIG. 4. Microtubule shrinkage velocity as a function of spastin concentration. Circles: average of at least three independent experiments each representing 30-100 MTs. Error bars show the standard deviation. Orange line: prediction of the herding model. Blue line: prediction if $\rho(0) = \rho_\infty$. v_0 was estimated from measurements with no spastin. v_1 is set to zero. Shaded regions represent 95% confidence intervals on $\overline{D}$, $\overline{k}$, and $\overline{c}$, which were estimated from direct measurements.

To compare predictions directly to the data, Fig. 4 shows the measured $v(c)$ values along with theoretical curves from our herding theory and for the case $\rho(0) = \rho_\infty$ (Langmuir kinetics without end enrichment). The shaded regions represent 95% confidence intervals for the parameter estimates. It is evident that Langmuir kinetics alone are insufficient to explain the measured slowdown, even for $\overline{v}_1 = 0$. The experimental data are all within the confidence bounds of the herding theory and it is clear that the theory is a good quantitative predictor of the measured shrinkage velocity.

Spastin's end-enrichment is likely to be biologically significant. According to experiments, a 50% slowdown in the shrinkage velocity is achieved at around 55 nM, which is close to the physiological concentration [32,33]. Without end-enrichment, this level of slowdown would be achievable only at much higher, micromolar concentrations (Fig. 4, blue curve). The slowdown at low solution concentration is due to a feedback effect: slowdown causes end enrichment and end enrichment in turn promotes slowdown. The high end occupancy driven by herding also has implications for spastin's regulation of the rescue frequency: although the precise mechanism of spastin's ATP-independent promotion of rescue is unclear, it is reasonable that the activity depends on an interaction with the shrinking end. For example, if spastin accelerates the binding of GTP-tubulin to the shrinking end, then its accumulation at the end can restore the GTP cap and thus the regrowth of that end.

Other applications. Although we have framed the herding theory in the context of regulatory proteins on shrinking polymers, the central principle is more general: particles that diffuse in a shrinking domain will enrich at the shrinking boundary if they hinder it. The essence of this effect is contained within a simplified version of the mean-field model,

$$\partial_t \rho = [1 - \rho(0, t)]\partial_x \rho + D\partial_x^2 \rho, \tag{6}$$

where the Langmuir kinetics are removed, $\overline{v}_1$ is set to zero, and D is a dimensionless diffusivity as defined in the SM
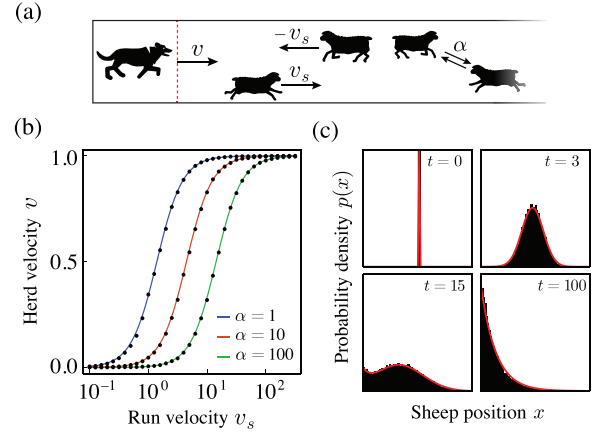

FIG. 5. Toy model of sheepherding. (a) Sheep are noninteracting run-and-tumble particles that hinder the sheepdog. (b) Average herd velocity v as a function of run velocity v_s and tumble rate α. Circles: simulation estimates. Lines: prediction of equation (7). $N = 5$. (c) Sheep position distribution at different times. Black bars: simulated histograms ($N = 1$). Red line: numerical solution of equation (7).

(Sec. II) [28]. Equation (6) serves as a generic theory of herding phenomena independent of any microscopic model. To illustrate this, and to motivate our terminology, we consider the following toy model of sheepherding [Fig. 5(a)]: a one-dimensional domain is bounded on one end by a sheepdog, which moves with velocity v_d in the positive direction when it is unimpeded. There are N sheep in the domain, each behaving as an independent run-and-tumble particle with run velocity v_s and tumble rate α. The sheep are reflected by the sheepdog, and the sheepdog pauses when there is a sheep within a length d ahead of it.

Numeric simulations suggest that this model is well described by equation (6) with the diffusivity set to $v_s^2/2\alpha$, which is the known effective diffusion coefficient for a run-and-tumble particle. With a reflecting boundary at $x = 0$ and the condition $\rho(\infty, t) = 0$, the stationary solution to equation (6) (SM, Sec. II) [28] predicts a steady-state herd velocity of

$$\frac{v}{v_d} = \frac{v_s^2}{v_s^2 + 2N\alpha v_d d}. \tag{7}$$

This result is in good agreement with simulations [Fig. 5(b)]. Time-dependent numeric solutions obtained via a nonlocal finite-difference scheme (SM, Sec. III) reveal that equation (6) is a nearly exact Fokker-Planck equation for the sheep position [Fig. 5(c)].

Conclusion. We have shown that a protein that slows a polymer's shrinkage will enrich near the shrinking end, leading to feedback between slowdown and end enrichment. This enrichment occurs even though the binding sites on the polymer are energetically equivalent. What drives the density distribution out of equilibrium is the polymer's shrinkage (Fig. 1), which breaks detailed balance and is dissipative. For microtubules, the energy source is GTP hydrolysis. For actin filaments, it is ATP hydrolysis [34], and for exonuclease-mediate DNA depolymerization it is nucleotide triphosphate hydrolysis. It is known that such processes

can generate mechanical work [35,36]; here, we show that they can also build protein density gradients with regulatory functions.

Our experiments demonstrate that the herding theory is a quantitative predictor of spastin's regulation of microtubule shrinkage and that direct binding and diffusive capturing are not necessary for end enrichment. We cannot rule out that processive tracking by oligomers is occurring in addition to herding [9,19]. Indeed, if oligomers slow depolymerization, then this will lead to herding.

Lastly, we showed how a simplified version of our mean-field model, equation (6), can describe more macroscopic herding phenomena. The dynamics described by equation (6) may arise in diverse contexts, including the motion of microtubule motors slowed by other MAPs [37] and the progression of DNA replication forks and RNA-polymerases hindered by DNA-binding proteins [38,39]. Outside of biology, such dynamics could arise in transport processes where a density buildup at the boundary slows the flow in the bulk, for example, the flow of a particle suspension through a filter.

[1] W. F. Marshall, How cells measure length on subcellular scales, Trends Cell Biol. **25**, 760 (2015).

[2] J. Howard and A. A. Hyman, Microtubule polymerases and depolymerases, Curr. Opin. Cell Biol. **19**, 31 (2007).

[3] P. Bieling, L. Laan, H. Schek, E. L. Munteanu, L. Sandblad, M. Dogterom, D. Brunner, and T. Surrey, Reconstitution of a microtubule plus-end tracking system in vitro, Nature (London) **450**, 1100 (2007).

[4] M. Edwards, A. Zwolak, D. A. Schafer, D. Sept, R. Dominguez, and J. A. Cooper, Capping protein regulators fine-tune actin assembly dynamics, Nat. Rev. Mol. Cell Biol. **15**, 677 (2014).

[5] E. Reithmann, L. Reese, and E. Frey, Nonequilibrium Diffusion and Capture Mechanism Ensures Tip Localization of Regulating Proteins on Dynamic Filaments, Phys. Rev. Lett. **117**, 078102 (2016).

[6] J. Helenius, G. Brouhard, Y. Kalaidzidis, S. Diez, and J. Howard, The depolymerizing kinesin MCAK uses lattice diffusion to rapidly target microtubule ends, Nature (London) **441**, 115 (2006).

[7] G. J. Brouhard, J. H. Stear, T. L. Noetzel, J. Al-Bassam, K. Kinoshita, S. C. Harrison, J. Howard, and A. A. Hyman, XMAP215 is a processive microtubule polymerase, Cell (Cambridge, MA, U. S.) **132**, 79 (2008).

[8] V. Varga, C. Leduc, V. Bormuth, S. Diez, and J. Howard, Kinesin-8 motors act cooperatively to mediate length-dependent microtubule depolymerization, Cell (Cambridge, MA, U. S.) **138**, 1174 (2009).

[9] G. A. Klein, K. Kruse, G. Cuniberti, and F. Jülicher, Filament Depolymerization by Motor Molecules, Phys. Rev. Lett. **94**, 108102 (2005).

[10] X. Chen, L. A. Widmer, M. M. Stangier, M. O. Steinmetz, J. Stelling, and Y. Barral, Remote control of microtubule plus-end dynamics and function from the minus-end, eLife **8**, e48627 (2019).

[11] F. J. McNally and A. Roll-Mecak, Microtubule-severing enzymes: From cellular functions to molecular mechanism, J. Cell Biol. **217**, 4057 (2018).

[12] A. Vemu, E. Szczesna, E. A. Zehr, J. O. Spector, N. Grigorieff, A. M. Deaconescu, and A. Roll-Mecak, Severing enzymes amplify microtubule arrays through lattice GTP-tubulin incorporation, Science **361**, eaau1504 (2018).

[13] Y. W. Kuo, O. Trottier, and J. Howard, Predicted effects of severing enzymes on the length distribution and total mass of microtubules, Biophys. J. **117**, 2066 (2019).

[14] Y. W. Kuo and J. Howard, Cutting, amplifying, and aligning microtubules with severing enzymes, Trends Cell Biol. **31**, 50 (2021).

[15] Y. W. Kuo, O. Trottier, M. Mahamdeh, and J. Howard, Spastin is a dual-function enzyme that severs microtubules and promotes their regrowth to increase the number and mass of microtubules, Proc. Nat. Acad. Sci. USA **116**, 5533 (2019).

[16] M. H. Hinrichs, A. Jalal, B. Brenner, E. Mandelkow, S. Kumar, and T. Scholz, Tau protein diffuses along the microtubule lattice, J. Biol. Chem. **287**, 38559 (2012).

[17] B. T. Castle, K. M. McKibben, E. Rhoades, and D. J. Odde, Tau avoids the GTP cap at growing microtubule plus-ends, iScience **23**, 101782 (2020).

[18] S. Y. Leong, T. Edzuka, G. Goshima, and M. Yamada, Kinesin-13 and kinesin-8 function during cell growth and division in the moss *physcomitrella patens*, Plant Cell **32**, 683 (2020).

[19] E. L. Grishchuk, Biophysics of microtubule end coupling at the kinetochore, Prog. Mol. Subcell. Biol. **56**, 397 (2017).

[20] G. M. Alushin, V. H. Ramey, S. Pasqualato, D. A. Ball, N. Grigorieff, A. Musacchio, and E. Nogales, The ndc80 kinetochore complex forms oligomeric arrays along microtubules, Nature (London) **467**, 805 (2010).

[21] V. A. Volkov, P. J. H. I. Veld, M. Dogterom, and A. Musacchio, Multivalency of Ndc80 in the outer kinetochore is essential to track shortening microtubules and generate forces, eLife **7**, e36764 (2018).

[22] S. Westermann, H. W. Wang, A. Avila-Sakar, D. G. Drubin, E. Nogales, and G. Barnes, The Dam1 kinetochore ring complex moves processively on depolymerizing microtubule ends, Nature (London) **440**, 565 (2006).

[23] S. M. Meier, A.-M. Farcas, A. Kumar, M. Ijavi, R. T. Bill, J. Stelling, E. Dufresne, M. O. Steinmetz, and Y. Barral, Multivalency ensures persistence of a +TIP body at specialized microtubule ends, Nat. Cell Biol. **25**, 56 (2023).

[24] V. A. Lombillo, R. J. Stewart, and J. R. McIntosh, Minus-end-directed motion of kinesin-coated microspheres driven by microtubule depolymerization, Nature (London) **373**, 161 (1995).

[25] H. Drechsler, Y. Xu, V. F. Geyer, Y. Zhang, and S. Diez, Multivalent electrostatic microtubule interactions of synthetic peptides are sufficient to mimic advanced map-like behavior, Mol. Biol. Cell **30**, 2953 (2019).

[26] A. B. Kolomeisky, G. M. Schütz, E. B. Kolomeisky, and J. P. Straley, Phase diagram of one-dimensional driven lattice gases with open boundaries, J. Phys. A: Math. Gen. **31**, 6911 (1998).

[27] A. Parmeggiani, T. Franosch, and E. Frey, Phase Coexistence in Driven One-Dimensional Transport, Phys. Rev. Lett. **90**, 086601 (2003).

[28] See Supplemental Material at http://link.aps.org/supplemental/10.1103/PhysRevE.107.L042601 for a detailed derivation of the analytic model, a table of parameter values, detailed experimental and numerical methods, and supplemental experiments on spastin's single-molecule kinetics. References [40–45] included therein.

[29] Y.-W. Kuo and J. Howard, In vitro reconstitution of microtubule dynamics and severingsevering imaged by label-free interference-reflection microscopy, in *Microtubules: Methods and Protocols*, edited by H. Inaba (Springer US, New York, 2022), pp. 73–91.

[30] Y. Tuna, A. Al-Hiyasat, and J. Howard, Simultaneous interference reflection and total internal reflection fluorescence microscopy for imaging dynamic microtubules and associated proteins, J. Vis. Exp. **183**, e63730 (2022).

[31] T. Eckert, D. T. V. Le, S. Link, L. Friedmann, and G. Woehlke, Spastin's microtubule-binding properties and comparison to katanin, PLoS ONE **7**, e50161 (2012).

[32] J. M. Solowska, G. Morfini, A. Falnikar, B. T. Himes, S. T. Brady, D. Huang, and P. W. Baas, Quantitative and functional analyses of spastin in the nervous system: Implications for hereditary spastic paraplegia, J. Neurosci. **28**, 2147 (2008).

[33] D. N. Itzhak, S. Tyanova, J. Cox, and G. H. Borner, Global, quantitative and dynamic mapping of protein subcellular localization, eLife **5**, e16950 (2016).

[34] Y. L. Wang, Exchange of actin subunits at the leading edge of living fibroblasts: possible role of treadmilling, J. Cell Biol. **101**, 597 (1985).

[35] D. E. Koshland, T. J. Mitchison, and M. W. Kirschner, Polewards chromosome movement driven by microtubule depolymerization in vitro, Nature (London) **331**, 499 (1988).

[36] M. Coue, V. A. Lombillo, and J. R. McIntosh, Microtubule depolymerization promotes particle and chromosome movement in vitro, J. Cell Biol. **112**, 1165 (1991).

[37] T. Korten and S. Diez, Setting up roadblocks for kinesin-1: Mechanism for the selective speed control of cargo carrying microtubules, Lab Chip **8**, 1441 (2008).

[38] V. Epshtein, F. Toulmé, A. R. Rahmouni, S. Borukhov, and E. Nudler, Transcription through the roadblocks: The role of RNA polymerase cooperation, EMBO J. **22**, 4719 (2003).

[39] G. M. Weaver, K. A. Mettrick, T. A. Corocher, A. Graham, and I. Grainge, Replication fork collapse at a protein-DNA roadblock leads to fork reversal, promoted by the RecQ helicase, Mol. Microbiol. **111**, 455 (2019).

[40] J. Schindelin, I. Arganda-Carreras, E. Frise, V. Kaynig, M. Longair *et al.*, Fiji: An open-source platform for biological-image analysis, Nat. Methods **9**, 676 (2012).

[41] M. Mahamdeh, S. Simmert, A. Luchniak, E. Schäffer, and J. Howard, Label-free high-speed wide-field imaging of single microtubules using interference reflection microscopy, J. Microsc. **272**, 60 (2018).

[42] C. Gell, V. Bormuth, G. J. Brouhard, D. N. Cohen, S. Diez *et al.*, Microtubule dynamics reconstituted in vitro and imaged by single-molecule fluorescence microscopy, Methods Cell Biol. **95**, 221 (2010).

[43] W. L. Deemer and D. F. Votaw, Estimation of parameters of truncated or censored exponential distributions, Ann. Math. Stat. **26**, 498 (1955).

[44] J. Bezanson, A. Edelman, S. Karpinski, and V. B. Shah, Julia: A fresh approach to numerical computing, SIAM Rev. **59**, 65 (2017).

[45] M. Castoldi and A. V. Popov, Purification of brain tubulin through two cycles of polymerization- depolymerization in a high-molarity buffer, Protein Expression Purif. **32**, 83 (2003).